Journal of Biomedical Optics

BiomedicalOptics.SPIEDigitalLibrary.org

Optical fiber sensors-based temperature distribution measurement in *ex vivo* radiofrequency ablation with submillimeter resolution

Edoardo Gino Macchi
Daniele Tosi
Giovanni Braschi
Mario Gallati
Alfredo Cigada
Giorgio Busca
Elfed Lewis

SPIE.

Optical fiber sensors-based temperature distribution measurement in *ex vivo* radiofrequency ablation with submillimeter resolution

Edoardo Gino Macchi,[a,*] Daniele Tosi,[b] Giovanni Braschi,[a] Mario Gallati,[a] Alfredo Cigada,[c] Giorgio Busca,[c] and Elfed Lewis[b]
[a]Università di Pavia, Dipartimento di Ingegneria Civile ed Architettura, via Ferrata 3, 27100 Pavia (PV), Italy
[b]University of Limerick, Optical Fibre Sensors Research Centre, Plassey House, Limerick, Ireland
[c]Politecnico di Milano, Dipartimento di Meccanica, via La Masa 34, 20158 Milano (MI), Italy

Abstract. Radiofrequency thermal ablation (RFTA) induces a high-temperature field in a biological tissue having steep spatial (up to 6°C/mm) and temporal (up to 1°C/s) gradients. Applied in cancer care, RFTA produces a localized heating, cytotoxic for tumor cells, and is able to treat tumors with sizes up to 3 to 5 cm in diameter. The online measurement of temperature distribution at the RFTA point of care has been previously carried out with miniature thermocouples and optical fiber sensors, which exhibit problems of size, alteration of RFTA pattern, hysteresis, and sensor density worse than 1 sensor/cm. In this work, we apply a distributed temperature sensor (DTS) with a submillimeter spatial resolution for the monitoring of RFTA in porcine liver tissue. The DTS demodulates the chaotic Rayleigh backscattering pattern with an interferometric setup to obtain the real-time temperature distribution. A measurement chamber has been set up with the fiber crossing the tissue along different diameters. Several experiments have been carried out measuring the space-time evolution of temperature during RFTA. The present work showcases the temperature monitoring in RFTA with an unprecedented spatial resolution and is exportable to *in vivo* measurement; the acquired data can be particularly useful for the validation of RFTA computational models. [DOI: 10.1117/1.JBO.19.11.117004]

Keywords: fiber optic sensors; distributed temperature sensor; radiofrequency thermal ablation; *ex vivo* liver tissue; Rayleigh backscattering.

Paper 140450R received Jul. 14, 2014; revised manuscript received Oct. 6, 2014; accepted for publication Oct. 8, 2014; published online Nov. 11, 2014.

1 Introduction

Pioneered through the 1990s as a therapy for hepatic tumors,[1,2] radiofrequency thermal ablation (RFTA) has rapidly been established as a clinical procedure for the treatment of kidney, lung, hepatic, and other types of tumors,[3–6] as well as for the correction of cardiac arrhythmia, pain management, and other types of cauterizations.[7] Unlike more invasive surgical procedures, or radiation/microwave ablation, RFTA is typically based on miniature percutaneously inserted devices, resulting in an outpatient procedure with a lower discomfort for the patients and the possibility to repeat the treatment over time. RFTA makes use of a midpower RF irradiance to generate a high-temperature field confined to the proximity of the RF-ablation device tip [active electrode (ae)]. Temperature values higher than 40°C to 44°C are cytotoxic for tumor cells: an exposure to 52°C for 60 s is considered a clinical reference value to guarantee tumor cells' mortality, while for temperature in excess of 60°C, cell death is nearly instantaneous.[8]

Performances and outcomes of RFTA are widely dependent upon the biological and electrical properties of the tissue undergoing ablation. In soft tissues, such as liver, whose main constituent is water, the electrical resistivity of the tissue quickly rises when the temperature reaches ~100°C due to the liquid-vapor phase change; this neutralizes the ablation process as the ablation device gets substantially insulated from the target tissue. This effect usually limits RFTA in liver to tumors 2 to 3 cm in diameter, nevertheless the use of multitined expandable probes, saline injection, and internal cooling of the device allows longer ablations and increases the size of treatable tumors.

The measurement of temperature at the ablation point is a key asset in RFTA, as temperature is both a key metric with a direct relationship to the tumor cells' mortality and an indicator of the physical phenomena occurring during ablation.

Infrared (IR) thermal imaging has been applied for bidimensional temperature measurement, achieving both good accuracy and high spatial resolution.[9,10] However, IR imaging is effective only in measurements performed on the surface of the tissue, as it requires a line of sight with the ablation point, and is not capable of detection at the point-of-care.

Sensors, both based on microelectromechanical systems (MEMS) and optical fibers, have been used for temperature measurement.[5] MEMS sensors are often installed on the ablation device or are externally inserted; recent developments allow the realization of MRI-compatible thermocouples, immune to the RF interference, and with sizes as low as 150-μm diameter. While easily meeting the temperature measurement accuracy required for thermal ablation monitoring (0.5°C to 1°C),[11] MEMS exhibits significant limitations: thermocouples are punctual sensors and allow a sensing density of ~1 sensor/cm^3 which is insufficient to map RFTA-induced temperature

*Address all correspondence to: Edoardo Gino Macchi, E-mail: edoardogino.macchi01@ateneopv.it

0091-3286/2014/$25.00

gradients often higher than 4°C/mm; they also exhibit a significant hysteresis due to typical response time of 2 to 5 s. Optical fiber sensors, particularly fiber Bragg gratings (FBGs),[12–14] have been successfully employed in thermal ablation.[11,14] With current state-of-the-art FBG fabrication, it is possible to fabricate FBGs on a drawing tower having a 80-μm diameter, 0.1 to 0.5-cm active length, ≪1s response time, and 1 FBG/cm sensing density on a single fiber. In 2014, Tosi et al.[15] have first demonstrated the possibility of using a linearly chirped FBG (LCFBG) as a distributed temperature sensor (DTS). The LCFBG has been applied to *ex vivo* RFTA monitoring, achieving a 75-μm resolution on a 1.5-cm length.

The present work aims at extending the thermal measurement in RFTA beyond the spatial resolution limitations, returning a complete monitoring of RFTA temperature distribution in real time during ablation. The measurement system consists of a DTS unit, based on Rayleigh backscattering measurement,[16,17] that estimates temperature with a submillimeter spacing capability. Compared with the LCFBG as in Ref. 15, the DTS allows recording distributed temperatures over several meters of fiber length, without separation between active and nonactive regions; on the other side, it involves a more complex interrogation than the spectrometric setup used for optical gratings as in Ref. 11–15. Several RFTA experiments have been carried out using medical-grade equipment for RF irradiance, performing ablation on *ex vivo* porcine liver confined in a chamber; the positioning of the sensing fiber allows detecting the whole radial temperature distribution along several diameters on the ablation plane, exploiting the long-sensing range of the DTS. The measurements' physical consistency is also verified by straightforward energy balance considerations. The DTS system determines the liver tissue temperature distribution with a very dense spacing allowing one to accurately record the strong spatial temperature gradients connected to RFTA. Such accurate measurements can be very useful for the precise validation of RFTA computational models and may allow for improving the understanding of the physics involved in the ablation procedure.

2 Setup

The measurement setup is depicted in Fig. 1. The RFTA setup is based on an RF generator (TAG 100W, Invatec, Roncadelle, Italy) working at 480 kHz; RF power is constantly monitored with an oscilloscope. The RF generator embeds an impedance-meter that measures the load impedance in real time and disconnects the RF power whenever it falls out of the 20- to 300-Ω range. The instantaneous values of electric potential V and electric current I are measured with an oscilloscope and used to compute the effective power W. A picture of the sensing setup is shown in Fig. 2(a).

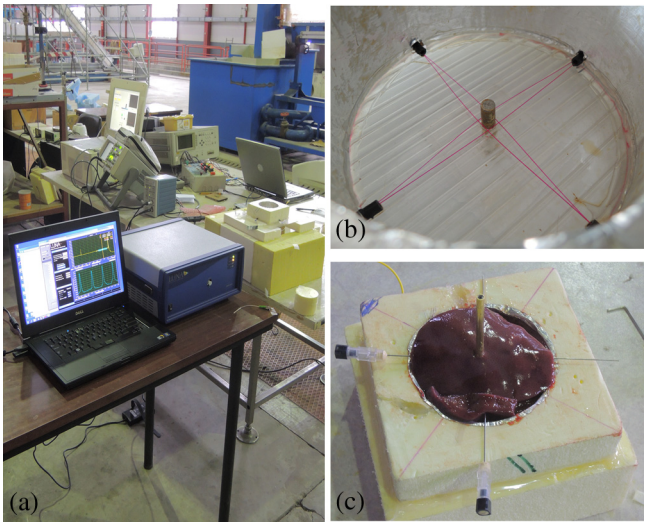

Fig. 2 Pictures of the experimental setup: (a) measurement setup, (b) experimental chamber—detail of the fiber positioning, and (c) one-dimensional (1-D) axisymmetric experimental chamber—the fiber is inserted into the tissue through medical needles.

Ablations have been performed *ex vivo* on porcine liver tissue since RFTA is most commonly used for the treatment of liver tumors. The liver specimens came from pigs slaughtered not more than two days earlier and were refrigerated until employed in the experiments.

The experimental chamber is shown in Fig. 1; it is a hollow cylinder (diameter 72 mm and height ∼60 mm) obtained from a block of extruded polystyrene foam, with a removable top cover; its inner lateral surface is covered with a thin metal sheet that acts as the ground (passive) electrode (pe). The ae is a stem-shaped hollow brass needle with 3/4 mm inner/outer diameter and 10-mm length; it is placed at the center of the base and is equipped with a temperature sensor. A second thermistor is

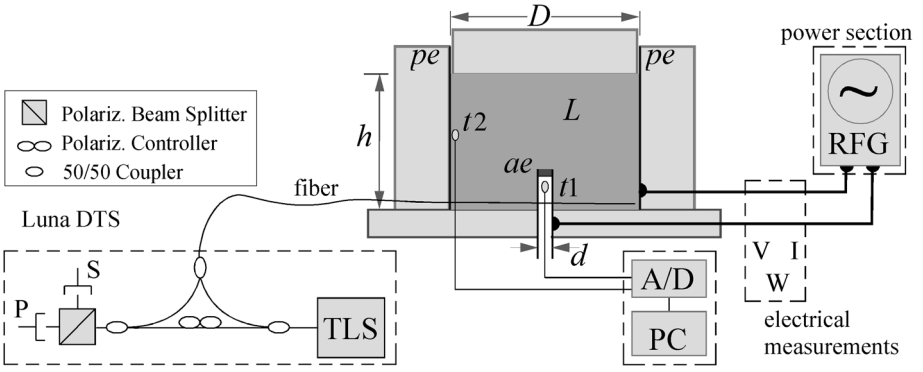

Fig. 1 Measurement setup. Luna distributed temperature sensor (DTS)—optical network used for polarization diverse measurement of Rayleigh backscatter; S, P: detectors, TLS: tunable laser source. Experimental chamber; L: liver tissue sample, ae: active electrode, pe: passive electrode, $d = 4$ mm (ae diameter), $D = 72$ mm (chamber diameter), $h = \sim 60$ mm (sample height), and $t1$, $t2$: reference thermistors.

positioned near the pe. In order to assure a proper placement of the fiber along several diameters, which is essential for fully exploiting the accuracy of the measurement system, the fiber is fixed to the chamber base before positioning the liver tissue sample. The fiber positioning inside the chamber is depicted in Fig. 2(b); the fiber has been colored to allow an easy identification. A single fiber coil travels inside and outside the measurement chamber, moving on the ablation plane over the 8 radii as shown in the photograph. In order to perform multiple passages along different radii, the fiber is bent outside the chamber using a long curvature radius (~8 cm) to prevent optical losses. Since the DTS measures the temperature changes, thermistor (B57861 Epcos, Munich, Germany; accuracy ±0.2°C) measurements are needed to initialize the absolute temperature.

In order to validate the physical consistency of the DTS measurements, a simpler setup for RF ablation is used: the ae length is now equal to the chamber height (52 mm in these experiments), making the phenomena one-dimensional (1-D) axisymmetric. In these experiments, the fiber is positioned inside the liver tissue (along two diameters of the test box) using small medical needles (outer diameter 0.4 mm), removed before starting the ablation [see Fig. 2(c)]. Also in these experiments, the fiber is bent outside the chamber. This also allows simulating a percutaneous insertion, preliminary examining the feasibility of DTS application during *in vivo* RF ablation.

The interrogation unit is a Luna OBR 4600 DTS, provided by Luna Technologies. The instrument is based on a swept-wavelength interferometry principle, as sketched in Fig. 1 and described in Ref. 16. A fiber-coupled tunable laser is launched into a fusion coupler, splitting the beam between the measurement arm (connected to the fiber installed in the experimental chamber) and a reference arm (internal to the instrument); a second coupler recombines the two arms. Using a polarization controller between the couplers, and a polarization beam splitter at the reference end, light is split into two orthogonal polarization states. DTS performances depend on a tight trade-off between accuracy, spatial resolution, and sampling time; by setting the measurement time to 1 s for the entire fiber length and choosing an accuracy estimated as 0.5°C, this configuration allows recording, with a minimum resolution of 200 μm in real time (and 20 μm in postanalysis with data processing), the amount of light backreflected in each portion of the fiber by Rayleigh scattering effect; this so-called Rayleigh signature is a chaotic pattern that maintains a high degree of stability when analyzed over a short fiber length (<20 m). When the fiber under test experiences a temperature increase, or is mechanically strained, it is possible to observe a red shift of the Rayleigh signature; typical coefficients are 10 pm/°C and 1.2 pm/$\mu\varepsilon$ at 1550 nm, similar to FBGs in glass fibers. By measuring the correlation between the reference and measured Rayleigh signatures for each portion of the fiber with a high computational speed, it is possible to obtain a distributed sensing pattern, whereas either temperature or strain is measured with a submillimeter spatial resolution. Figure 3 shows the principle of operation of the DTS during operation. The instrument detects the Rayleigh backscattering pattern along the whole fiber length, whereas the red portion of the fiber is selected and calibrated; thus, in real time, the instrument returns the instantaneous temperature change with the spatial resolution selected beforehand. The instrument used is an improved version of the system investigated about 10 years

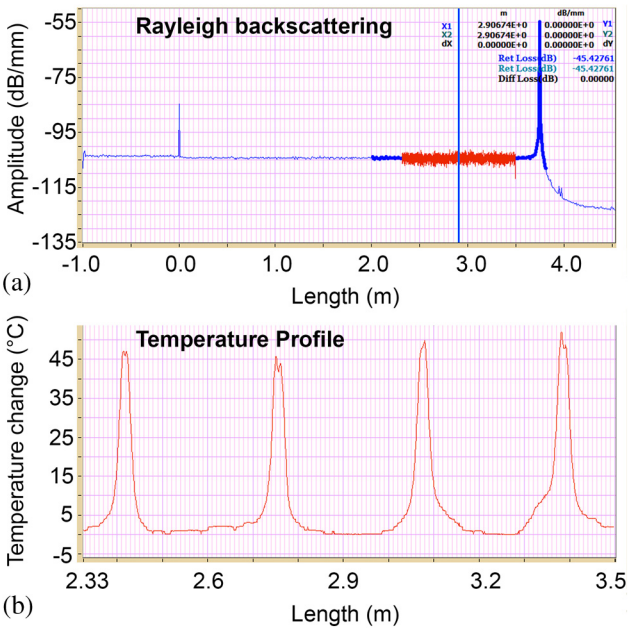

Fig. 3 Outline of the DTS measurement. (a) The backscattering pattern along the whole fiber length, showing a backreflection peak at the fiber connector (0 m) and a strong backreflection at the uncleaved fiber end (3.7 m). The red portion (2.33 to 3.50 m) of the sensing fiber contains the fiber exposed to radiofrequency thermal ablation (RFTA) and is further processed, estimating the Rayleigh signature and consequently the temperature variation (b). The four different peaks correspond to the different portions of fiber "crossing" the liver tissue and exposed to ablation.

ago by Gifford et al.[16] It can perform temperature measurements with very high-spatial resolution (up to 20 μm) and accuracy. The measurement accuracy is directly connected to the desired spatial resolution: the technical specifications for 0.2 mm resolution report a 0.5°C accuracy; this is more than adequate to capture the temperature distribution produced by RFTA. Several RFTA experiments have been performed choosing a spatial resolution of 0.2 mm for real-time operation; resolution has been chosen as a trade-off with sampling rate (1 Hz, approximately) and active fiber length. A "virtual" 20-μm spacing may be achieved by resampling the whole Rayleigh backscattering pattern through postanalysis computations.

The DTS system has a typical cost higher than the RFTA equipment itself; however, it makes use of an inexpensive standard single-mode fiber as the sensor, with only the requirement of a clean end surface, making it suitable for a disposable use paired with a disposable RFTA device. In most experiments, a standard single-mode SMF-28 fiber standard is used without capillary/catheter enclosing; despite the absence of protective elements, the fiber performed accurate linear sensing up to over 120°C without perceivable detuning due to strain. This was preliminary tested comparing measurements along the same diameter with and without a capillary enclosure. The DTS is precalibrated using a test fiber with ~100% backreflection on its end prior to all the measurements. Before each individual experiment, the Rayleigh signature is acquired with the fiber positioned in the setup as in Figs. 1 and 2, before activating the RF generator; hence in homogeneous temperature conditions, thermistors are used to initialize the absolute temperature starting value.

3 Experimental Results

The previously described measurement setup [Figs. 1, 2(a), and 2(b)] has been used to perform RF ablations at 15-W power. For each experiment, eight radial temperature distributions are acquired. As an example, the temperature space-time evolution along each radius of an experiment is plotted in Fig. 4. Data are reported in thermal map format, reporting the instantaneous temperature as a function of time elapsed and distance from the ablation tip, in a three-dimensional chart that shows the temperature distribution as well as the symmetry of the ablation pattern. In the proximity of the ae, temperature exhibits a rapid growth, overcoming the 60°C threshold within the first minute. After this initial rise, the heating rate slows down, reaching a plateau around 95°C to 100°C, whereas the water constituent of the tissue approaches the boiling temperature. As the liquid-vapor phase change takes place, the electrical load impedance rises and RF power is suspended when the impedance exceeds the 300-Ω threshold; after this event, the tissue rapidly cools down.

The similarity of these measurements is evident; only during the liquid-vapor phase change, the less deterministic part of the RFTA procedure, differences between different radii are observed. These differences are particularly significant just before the automatic power suspension when vapor completely surrounds the ae forming a large vapor bubble that rapidly expands, deforming the tissue. In addition, the tissue heterogeneities might also cause a slight asymmetry of the temperature field due to hot liquid or vapor escape through the tissue microvasculature. Anyway, these artifacts only appear only before power suspension when the procedure is almost finished.

In order to account for the intrinsic variability of biological tissue, this RFTA test was repeated four times. The RFTA procedure durations were respectively 259, 274, 258, and 239 s. For each experiment, the measured temperature distributions are averaged obtaining an average radial temperature distribution. For each of the four repeated experiments, the evolution of the average temperature distribution is depicted in Fig. 5. As expected, differences between experiments are noticed mainly during the vaporization. Averaging once more, we deduce an overall average temperature distribution characteristic for this type of RF ablation. The overall temperature space-time evolution, computed using all 32 radial temperature distributions, is plotted in Fig. 6(a), where time has been normalized for the total duration of the heating procedure.

The analysis of the thermal maps allows verifying the consistency of the recorded data: the temperature spatial and temporal evolutions are smooth and reasonably correct from a physical point of view.[10] The overall temperature distribution at different times is plotted in Figs. 6(b) and 6(c), respectively, during power supply and after the power suspension. Figure 7 depicts the temperature history of points at different distances from the ae (solid lines) together with the temperature measurement inside the electrode performed with an NTC thermistor (dashed line). The two different temperature measurements are almost identical: this confirms the accuracy of the Luna DTS measurements. The overall temperature distributions are representative of the performed ablations; this is highlighted in Fig. 8 which compares the overall distribution (solid line) at different times and the average distributions of each experiment (markers). As expected from experiments on biological tissue, despite the good agreement obtained during heating, the temperature differences between different experiments can be considerably higher (up to ~3°C) than the measurement accuracy (Fig. 8).

The temperature space-time evolution of two 1-D axisymmetric experiments is depicted in Fig. 9(a). The previously described averaging procedure has also been applied to these tests. The applied power can be computed differentiating the energy, deduced by integrating the temperature distributions

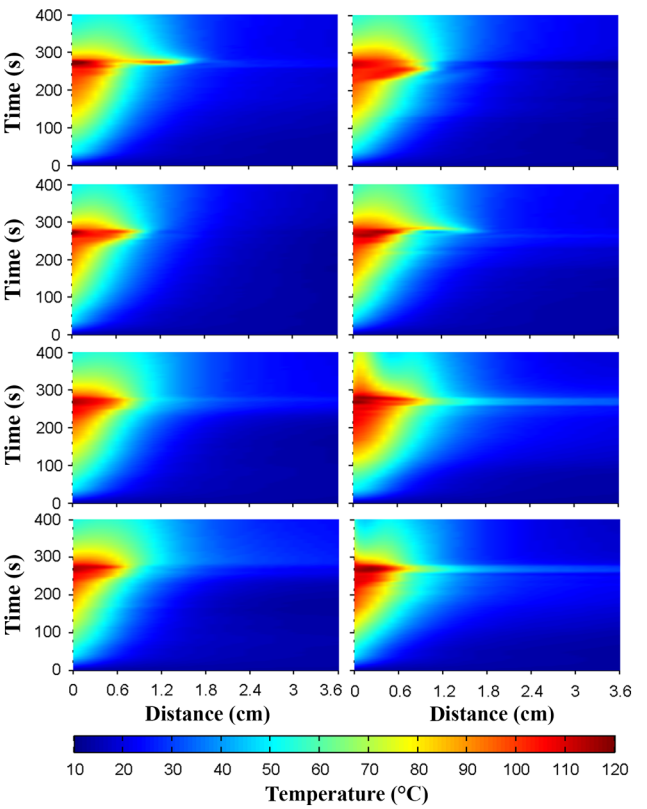

Fig. 4 Temperature space-time evolution during RFTA along eight different radii. For each radius, temperature is reported as a colormap as a function of distance from ablation tip (considered on the 0- to 3.6-cm interval) and time elapsed. A remarkable similarity between the radii is observed during heating, while during the phase change an asymmetry is noticed.

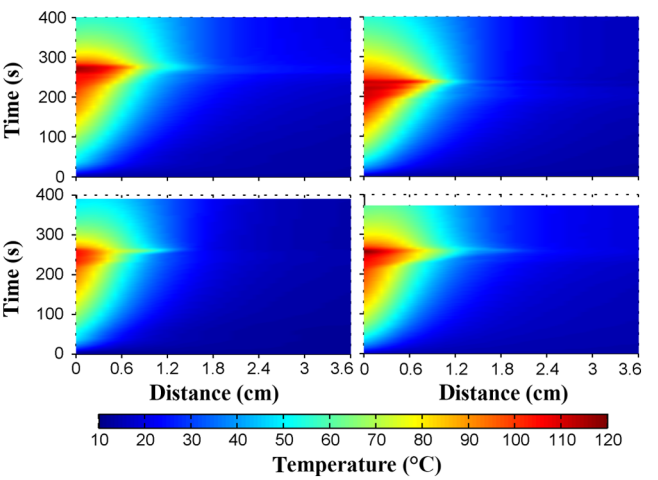

Fig. 5 Average temperature space-time evolution for each repeated experiment.

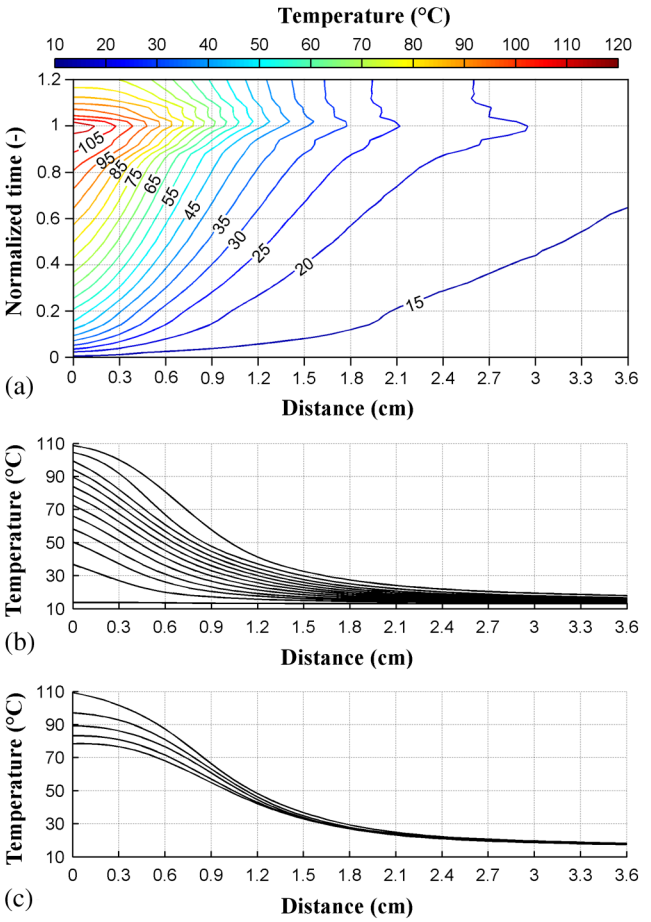

Fig. 6 Overall temperature distribution: (a) space-time evolution; (b, c) radial distribution at different times (time step 20 s) during power supply and during cooling. This information is representative of the performed RF ablations.

over space, with respect to time. The computed time histories of energy and power during heating are depicted in Fig. 9(b) together with the average power. The difference between the computed average power and the power set in the generator is below 3%, which further confirms the physical consistency of the DTS measurements. The data from such an experiment could also be used to numerically compute the energy balance starting from the measured space-time temperature evolution.

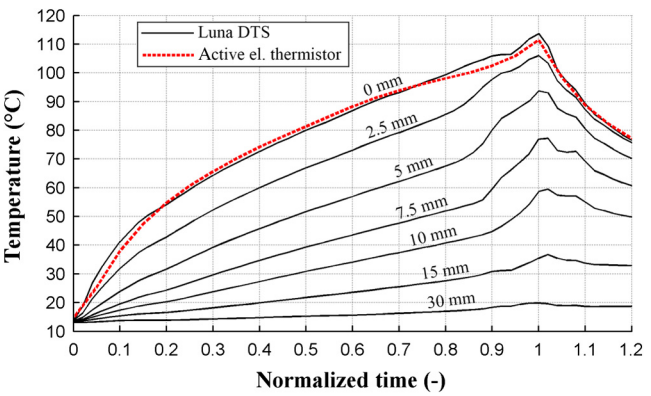

Fig. 7 Temperature history of points at different distances from ae (solid line) and ae thermistor measurement (dashed line).

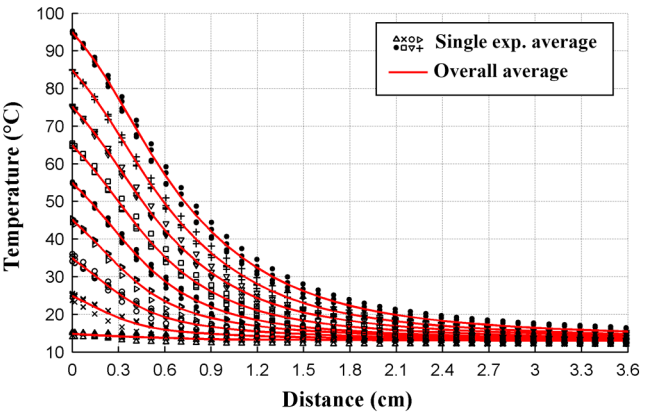

Fig. 8 Radial temperature distributions during heating: overall average (solid line) and single experiment average (markers). Despite experiments performed on biological tissue are usually characterized by high variability, the average distributions from each experiment (markers) are in good agreement (maximum temperature differences ~3°C).

4 Discussion

The DTS system allows recording temperature at the RFTA point of care with ultradense resolution, allowing a precise recording of the steep temporal and spatial gradients induced by RFTA. In addition to the increase of sensing density, the Rayleigh-based system behaves as a continuous chain of punctual sensors, with an active length as long as the spatial resolution. In view of the measurement results, the DTS evolves the thermal measurement from a discrete set of points, each resulting as a spatial averaging, to a continuous distribution of points with negligible averaging; it shows a better response to minute thermal events occurring in the tissue and provides a quantitative estimation of the ablation pattern symmetry. The comparison of DTS with other measurement techniques applied to RFTA shows a significant improvement in measurement quality. While MEMS sensors provide the punctual measurement, FBGs provide an inline measurement along a discrete number of sensing points, achieving a density of 1 sensor/cm on a single channel. The work recently presented by Tosi et al.[15] extends from single-point or multipoint sensing to distributed sensing using LCFBG; this approach, however, is limited to the active region of the LCFBG (1.5 cm in Ref. 15, and up to 3 to 5 cm with improved fabrication facilities) and is highly dependent on a detection algorithm that discriminates each local temperature. The use of a DTS system provides another significant step forward in RFTA monitoring, as it makes the measurement entirely distributed using the entire fiber link as an active sensor and having the estimation of each local temperature virtually independent of the spatially adjacent values. The present work emphasizes the value of a distributed measurement system that can record the temperature along several ablation axes with a single fiber and a single channel. The proposed sensing setup, outlined in Figs. 1 and 2, provides an effective benchmark for the evaluation of thermal ablation procedures in phantoms and can be exported to other types of biological tissues, as well as other ablation sources (e.g., microwave and laser).

With the emerging of thermal ablation, one of the main challenges is the development of a biophysical model that supports ablation and can drive interventional procedures such as RFTA. For hepatic tumors, European FP7 IMPPACT project[18] has provided a sound imaging-based model of RF ablation. However,

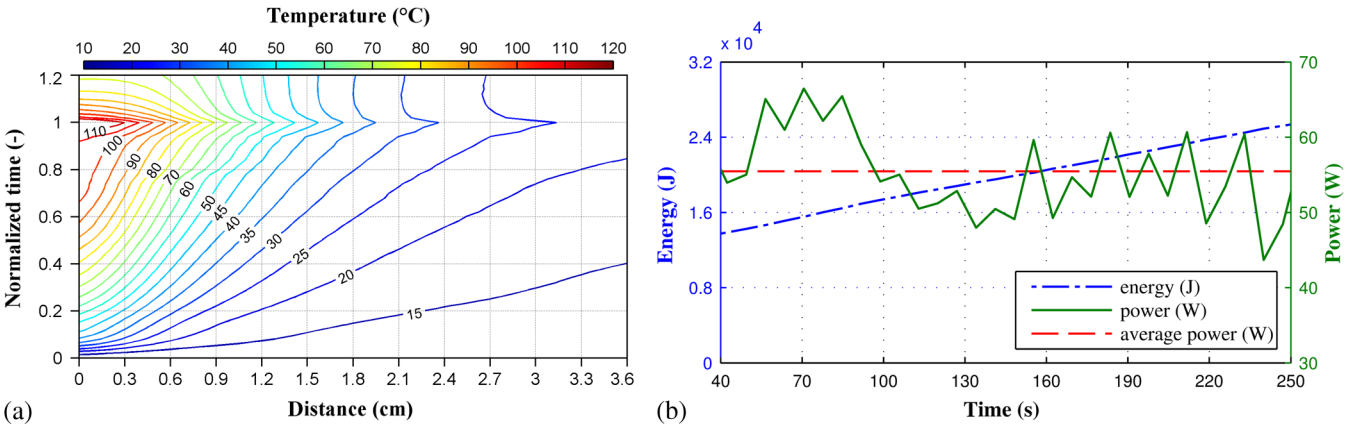

Fig. 9 Results of 1-D axisymmetric experiments simulating *in vivo* insertion: (a) overall temperature space-time evolution; and (b) energy and power time histories computed from DTS measurements.

the validation of such models is fundamental: up to now only thermal lesion measurements and a few spot temperature measurements (usually performed with thermocouples) have been used for this purpose. This is insufficient because of the steep spatial gradients, in particular for *in vivo* situations that are generally characterized by an asymmetric temperature field due to tissue heterogeneities and to the presence of large blood vessels. The DTS appears to be particularly useful for research purposes: its accurate and dense temperature distribution measurements can be employed for closely investigating the physics of RF ablation and for the validation of thermal ablation models. Future work will focus on upgrading the standard RFTA mathematical model progressing toward sensor-driven models, where several hundred sensing points are included in the analysis.

A final consideration is for the applicability of the DTS *in vivo*. The DTS makes use of a single-mode fiber, biocompatible and suitable for disposable use, as the sensor. The fiber can either be installed on the ablation device or introduced externally, penetrating the tissue using a catheter. Using 80-μm fibers, or the latest 40- to 60-μm fibers, it is possible to minimize the occupation and the alteration of the RFTA trace; it is also possible to interrogate different channels in a time-multiplexing scheme. The DTS only measures the temperature change; although body temperature is known the use of a standard sensor to initialize the temperature should be preferred. The main barrier toward *in vivo* application is the strong backreflection occurring at the fiber end, which is several orders of magnitude stronger than the Rayleigh signature and overcomes the temperature estimation in the portion of the fiber close to its tip, which corresponds to the active part of the ablation. As a consequence, the measurement is inaccurate within a 1 to 2 cm region from the fiber endpoint if the perfect cleave of the fiber end is not guaranteed. A possible solution to this problem is to insert the fiber through a microcatheter that sustains the penetration in the tissue, and then to remove it leaving the fiber in place while preserving the quality of the fiber end surface. The results of such an experiment, simulating an *in vivo* insertion of a fiber sensor in the tissue, are shown in Fig. 9. RFTA is performed under ultrasound guidance or MRI: with external insertion, the correct positioning of the fiber (protected by a catheter) is possible, however, an objective positioning of the sensor, relative to the ablation device may not be guaranteed. On the other hand, by embedding the sensor on the ablation device, each temperature data recorded has a univocal positioning with respect to the active part of the RFTA device; however, this approach is sustainable only if the fiber remains protected in a catheter which partially absorbs temperature and alters the response of the fiber sensor to thermal variations making the distributed measurements less meaningful.

A possible alternative to this problem is the use of the novel all-grating fibers (AGFs),[19] in conjunction with an interferometric setup similar to the one proposed in Fig. 1. Thanks to draw-tower fabrication, it is possible to fabricate a continuous set of weak FBGs (reflectivity ~0.1%) in a single-mode fiber. The wavelength-selective behavior of FBGs has the key advantage of being almost independent of broadband reflections, such as the one occurring at the fiber tip; as a result, AGF-based systems are more tolerant to *in vivo* fiber insertion. On the other hand, the typical spatial resolution, as well as the active length of each sensing point in AGF systems is 0.5 to 1.0 mm, providing a one order of magnitude improvement over FBG arrays but still being up to one order of magnitude far from a DTS. The possibility of detecting the ablation pattern during the RFTA in real time is a key asset for a "smart-ablation" concept, where thermal data can drive the treatment as well as provide key indicators of events related to ablation; the latest developments in ultradense fiber-optic distributed sensors can open new frontiers in this direction, expanding sensing capabilities from three to five points such as those in the latest RFTA devices to hundreds of sensing points along a few centimeters length.

5 Conclusions

Thermal field measurements during RFTA on *ex vivo* liver tissue have been presented. The sensing setup is based on a Luna OBR4600 unit that exploits Rayleigh backscattering to measure the temperature distribution with very dense submillimeter spacing (up to 20 μm). Four RF ablation experiments have been performed, measuring the temperature distribution along eight different radii. The average temperature space-time evolution obtained from 32 measured radial distributions has been employed to check the data's physical consistency and accuracy. The results of preliminary RF ablations simulating *in vivo* insertion are also presented. The reported measurements can be employed for closely investigating the physics of RF ablation and for the validation of RFTA models. These results, which partially overcome the previous RFA literature, set the basis for distributed temperature monitoring during thermal ablation.

Acknowledgments

The present work has been financially supported by Marie Curie IEF action (MC-IEF-299985) and Ordine degli Ingegneri della Provincia di Pavia; research has been supported by Fondazione per la Cura Mini-Invasiva dei Tumori. The authors acknowledge the contribution of Maurizio Chiani and Ian Shannan for providing and setting up the DTS unit for RFTA experiments.

References

1. S. Rossi et al., "Percutaneous RF interstitial thermal ablation in the treatment of hepatic cancer," *Am. J. Roentgenol.* **167**(3), 759–768 (1996).
2. L. Buscarini and S. Rossi, "Technology for radiofrequency thermal ablation of liver tumors," *Surg. Innovation* **4**(2), 96–101 (1997).
3. S. N. Goldberg, G. S. Gazelle, and P. R. Mueller, "Thermal ablation therapy for focal malignancy: a unified approach to underlying principles, techniques, and diagnostic imaging guidance," *Am. J. Roentgenol.* **174**, 323–331 (2000).
4. L. Solbiati et al., "Percutaneous radio-frequency ablation of hepatic metastases from colorectal cancer: long-term results in 117 patients," *Radiology* **221**, 159–166 (2001).
5. M. J. Dodd, "Radiofrequency ablation of the liver: current status," *Am. J. Roentgenol.* **176**, 3–16 (2001).
6. S. Padma, J. B. Martinie, and D. A. Iannitti, "Liver tumor ablation: percutaneous and open approaches," *J. Surg. Oncol.* **100**, 619–634 (2009).
7. U. Halm et al., "Thermal esophageal lesions after radiofrequency catheter ablation of left atrial arrhythmias," *Am. J. Gastroenterol.* **105**(3), 551–556 (2010).
8. S. A. Sapareto, "Thermal dose determination in cancer therapy," *Int. J. Radiat. Oncol., Biol., Phys.* **10**(6), 787–800 (1984).
9. K. Ogan et al., "Infrared thermography and thermocouple mapping of radiofrequency renal ablation to assess treatment adequacy and ablation margins," *Urology* **62**, 146–151 (2003).
10. E. G. Macchi et al., "Temperature distribution during RF ablation on ex vivo liver tissue: IR measurements and simulations," *Heat Mass Transfer* (2014).
11. P. Saccomandi, E. Schena, and S. Silvestri, "Techniques for temperature monitoring during laser-induced thermo-therapy," *Int. J. Hyperthermia* **29**, 609–619 (2013).
12. A. Othonos and K. Kalli, *Fiber Bragg Gratings: Fundamentals and Applications*, Artech House, Boston (1999).
13. V. Mishra et al., "Fiber grating sensors in medicine: current and emerging applications," *Sens. Actuators A* **167**, 279–290 (2011).
14. F. Taffoni et al., "Optical fiber-based MR-compatible sensors for medical applications: an overview," *Sensors* **13**, 14105–14120 (2013).
15. D. Tosi et al., "Fiber-optic chirped FBG for distributed thermal monitoring of ex-vivo radiofrequency ablation of liver," *Biomed. Opt. Express* **5**(6), 1799–1811 (2014).
16. D. K. Gifford et al., "Distributed fiber-optic temperature sensing using Rayleigh backscatter," *ECOC Proc.* **3**, 511–512 (2005).
17. M. E. Froggatt et al., "Characterization of polarization-maintaining fiber using high-sensitivity optical-frequency-domain reflectometry," *J. Lightwave Technol.* **24**(11), 4149–4154 (2006).
18. FP7 IMPPACT Project, 2011, www.imppact.eu (27 October 2014).
19. N. Liu et al., "Directional bend sensing with Bragg gratings in all solid Bragg fibers," *IEEE Photon. Technol. Lett.* **23**(17), 1237–1239 (2011).

Edoardo Gino Macchi is a PhD student at the University of Pavia. He received his BEng degree (workplace and environmental safety engineering) from Insubria University in 2008, and the MEng (environmental engineering) degree from University of Pavia in 2011. His research interests include radiofrequency ablation of tumors, heat, and mass transport in porous media, and CFD.

Daniele Tosi is a Marie Curie Intra-European Fellow at the University of Limerick. He received his BEng, MEng (telecommunication engineering), and PhD degrees (electronic engineering) from Politecnico di Torino in 2004, 2006, and 2010, respectively. His research activity includes fiber-optic pressure sensors, fiber Bragg gratings, and signal processing.

Giovanni Braschi has been an assistant professor at the University of Pavia since 1981, where he teaches geotechnics. His research activity is now focused on radiofrequency thermal ablation of tumors and heat and mass transport in porous media. He also studied more classical civil engineering problems (e.g., seepage, flooding, landslides) developing ad-hoc codes based on Eulerian and Lagrangian numerical methods (e.g., finite volumes, vortex method, smoothed particle hydrodynamics).

Mario Gallati has been a professor of hydraulics and fluid mechanics at the University of Pavia since 1984. His research experience includes seepage, free surface flows, flood and shock wave propagation in rivers and urban environments, heat and mass transport in porous media. From 2005, his research activities are focused on improving physical understanding and efficacy of radiofrequency thermal ablation of liver tumors through a combined experimental and numerical approach.

Alfredo Cigada is a professor of mechanical and thermal measurements since 2002 at Politecnico di Milano and Università di Pavia (2003 to 2008). He has about 180 papers in the following topics: fluid-structure interaction, vehicle substructure interaction, electromechanical interaction, image processing, new measurement techniques, especially with new sensors (MEMS and fiber optics), acoustics, structural health monitoring and liver tumor radiofrequency thermal ablation. He has been coordinator or principal investigator of several EU and national projects.

Giorgio Busca received his PhD degree in mechanical system engineering in 2011 and now is working as a postdoctoral research fellow at Politecnico di Milano. He is an author of many papers on topics about mechanical measurements. His main research activity is focused on imaging processing applied to mechanical issues and data analysis for damage detection in the field of structural health monitoring.

Elfed Lewis is an associate professor and director of the Optical Fibre Sensors Research Centre, which he founded in 1996. He has authored and coauthored more than 70 journal papers and made in excess of 200 contributions to international conferences. The Optical Fibre Sensors Research Centre under his leadership is engaged in investigating sensors for environmental monitoring, food quality assessment, and parameters of high-power microwave sources and medical devices.